Microdiffraction Experiments on Single Polymeric Fibers by Synchrotron Radiation

C. Riekel,* A. Cedola, F. Heidelbach, and K. Wagner

European Synchrotron Radiation Facility, B. P. 220, F-38043 Grenoble Cedex, France

Received June 3, 1996; Revised Manuscript Received October 23, 1996[⊗]

ABSTRACT: It is shown that wide-angle X-ray scattering patterns can be obtained from single polymeric fibers with a 2 μm synchrotron radiation beam in a few seconds per pattern. Preferred orientation was observed for an ultrahigh molecular weight polyethylene fiber where orthorhombic plus monoclinic phases were found to coexist in the outer parts of the fiber. For a poly(*p*-phenyleneterephthalamide) fiber (Kevlar 49) the radial sheet model was verified, but an important texture appears to be present.

Introduction

X-ray beam sizes down to the micron range and smaller have been demonstrated with glass capillary optics at synchrotron radiation (SR) sources.[1,2] The high monochromatic flux which can be obtained at an undulator beam[3,4] can be used for wide angle X-ray scattering (WAXS) experiments on single polymeric fibers with diameters down to a few microns in a few seconds per image. In contrast to single fiber SR experiments with a beam larger than the sample diameter,[5,6] scanning experiments become thus feasible. Microdiffraction laboratory WAXS experiments on single fibers require for comparison a few hours per pattern.[7] As compared to transmission electron diffraction (TEM), which requires even thinner samples and special preparation techniques which may introduce artifacts, no special treatment is required for WAXS experiments and samples can be kept in air. In addition, model calculations based on kinematic scattering theory are straightforward. These points are demonstrated in this article for ultrahigh molecular weight (UHMW) polyethylene (Dyneema) and poly(*p*-phenyleneterephthalamide) (Kevlar 49) fibers.

Experimental Section

UHMW polyethylene and Kevlar 49 fibers were obtained from Goodfellow Cambridge Ltd. The molecular weight was determined for polyethylene as $M_w = 1.4 \times 10^6$. Individual fibers were selected under a microscope and glued to 1 mm diameter electron microscopy apertures. Prior to experiments, individual fibers were imaged by a scanning electron microscope (SEM) after shadowing with gold.

Synchrotron radiation experiments were performed at the microfocus beamline of the European Synchrotron Radiation Facility (ESRF).[8] The experimental setup is shown in Figure 1. A monochromatic X-ray beam of 0.96 Å with a flux of $\approx 10^{10}$ photons/s at 100 mA ring current was obtained by a combination of a Si-111 monochromator, ellipsoidal mirror, and tapered glass capillary. The beam size was determined to be about 2 μm (full width) at the capillary exit by scanning a knife edge into the beam and recording the intensity with a photodiode. Figure 2 shows the relative intensity as a function of the position of the knife edge. The fit corresponds to a 2 μm diameter disk with rounded edges. Several experiments were also performed with a 10 μm platinum aperture at the exit of the capillary in order to reduce background scattering from the capillary.[9] Due to the larger distance of the sample from the capillary exit, the beam size at the sample position was ≈ 5 μm in this case. For unit cell determination on single fibers, complimentary experiments were performed with a 30 μm beam from a collimator at $\lambda = 0.6889$ Å. The flux was in this case $\approx 10^{12}$ photons/s.

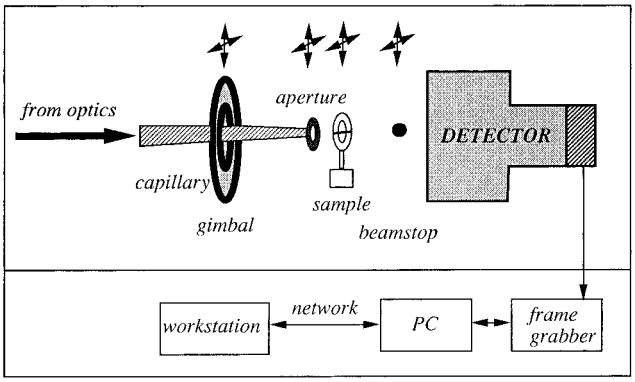

Figure 1. Experimental setup of the microfocus wide-angle X-ray scattering experiment. Motorization of components is indicated schematically by arrows.

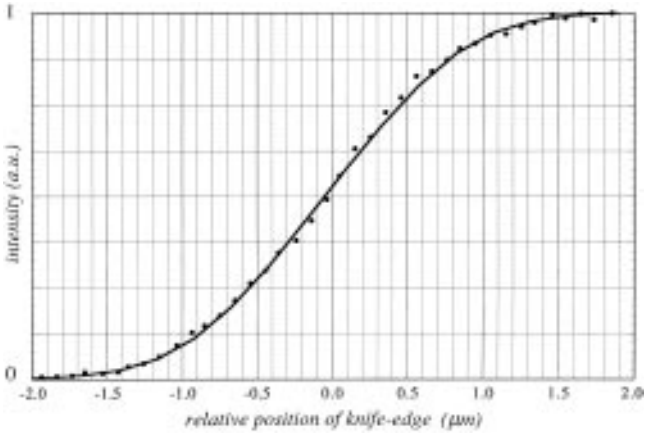

Figure 2. Determination of the beam profile by scanning a knife edge through the beam. Intensity is scaled to 1 for the knife edge out of the beam.

The sample holder was fixed on a goniometer head and the fiber axis was aligned optically in the horizontal plane. For scanning experiments with the 2 μm beam, goniometer head and sample could be translated into two orthogonal directions with an absolute accuracy of ≤ 1 μm. A 300 μm diameter beamstop was placed at ≈ 10 mm from the sample. A Photonics Science LA detector with video readout and on-line digitization and integration by a Synoptics Sprynt board was used for data collection.[10] The sample to detector distance was ≈ 100 mm. Fibers were aligned in the X-ray beam by watching the appearance of the diffraction pattern in real time on a video screen while the sample was translated through the beam. Typical integration times per WAXS pattern were 8 s. Experiments were performed by selecting discrete positions across a

[⊗] Abstract published in *Advance ACS Abstracts,* January 1, 1997.

S0024-9297(96)00799-1 CCC: $14.00

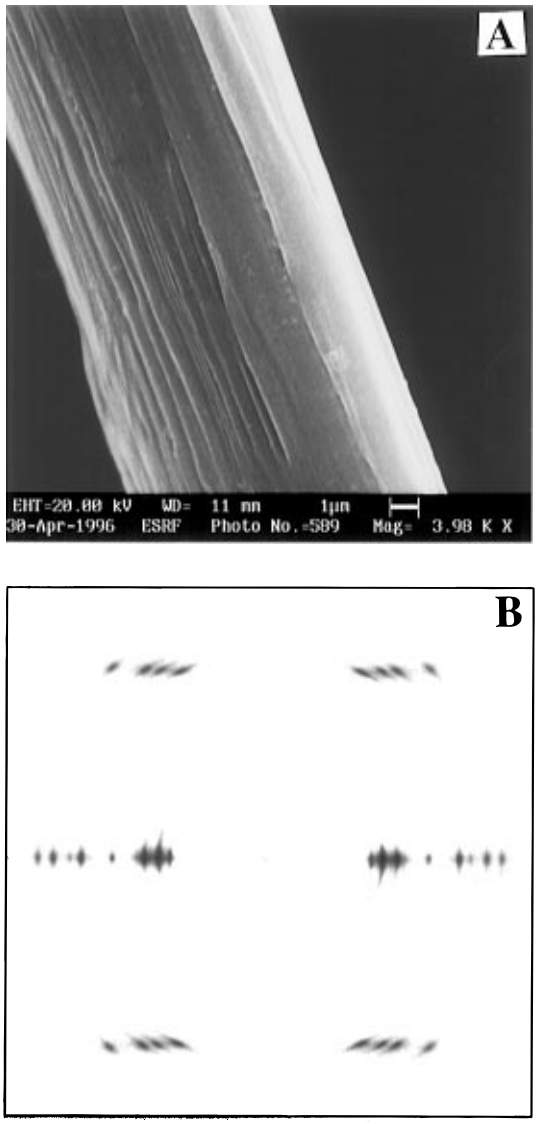

Figure 3. (a) Scanning electron microscopy (SEM) image of a polyethylene fiber. (b) WAXS pattern of a polyethylene fiber (logarithmic scale); the fiber axis is vertical.

fiber but also in the scanning mode. WAXS patterns were not modified during data collection which suggests that radiation damage was negligable. For experiments with the 30 μm beam, the goniometer head with sample was placed on a K-goniometer. The fiber was aligned with the help of a long distance microscope. For data collection, a 300 mm MAR research image plate system was used. The distance sample to detector was 378 mm. Diffraction patterns were calibrated by an Al_2O_3 standard. For data display and data reduction the software package FIT2D was used.[11]

Results and Discussion

UHMW Polyethylene: An SEM image of a ≈20 μm thick polyethylene fiber is shown in Figure 3a. A WAXS pattern, recorded with the 30 μm beam, corresponds principally to the fiber diffraction pattern of orthorhombic polyethylene (Figure 3b).[7,12] The peak count rate of the strongest reflection (110) is about 2500 counts/s. The unit cell was determined as $a = 7.38(1)$ Å, $b = 4.96(3)$ Å, $c = 2.57(2)$ Å. No evidence for a texture was found as the pattern was not modified upon rotating the sample around the fiber axis. Depending on the rotation up to two weak equatorial reflections of a further phase were observed with d values of $d = 4.68$ Å and $d = 3.92$ Å. These are compatible with the $(010)^t/(100)^t$ reflections of a triclinic[13] or the $(001)^m/(200)^m$ reflections of a monoclinic phase.[14] In the subsequent text, these reflections will be assigned to the more refined monoclinic phase model. Figure 4 shows part of the measured equatorial pattern, the pattern obtained by fitting 2D Gaussian profiles and a polynomial background to the peaks and the difference pattern. It is evident that azimuthal broadening due to chain disorder and an amorphous halo due to amorphous zones[15] are not properly taken into account by this model.

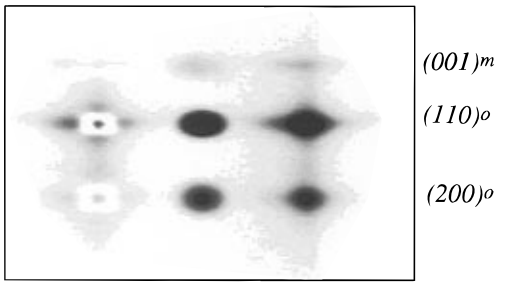

Figure 4. Part of the equatorial pattern of the polyethylene fiber (logarithmic scale; cut at 10% of maximum intensity in order to show weak intensities); right column, experimental pattern; middle column, fitted pattern; lower column, difference pattern.

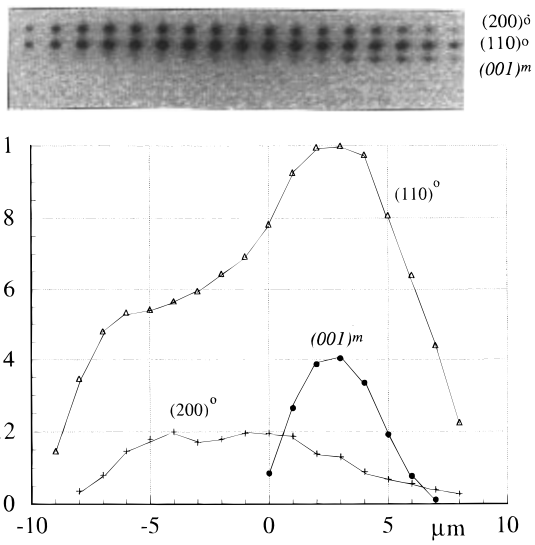

Figure 5. (a) Composite equatorial WAXS patterns obtained in the radial direction from a polyethylene fiber with a 5 μm beam. Individual pattern recorded in 8 s; step increment, 1μm; the fiber axis is horizontal. (b)Variation of integrated intensity of orthorhombic (^{o}) and monoclinic (^{m}) polyethylene reflections for 1 μm steps radially across the fiber with a 2 μm beam. Solid lines are guide lines for the eye (also for the following figures).

Figure 5a shows a composite of equatorial WAXS patterns which were obtained by scanning the fiber through the 5 μm beam with a step width of 1 μm in order to allow for oversampling. All patterns show the $(110)^o/(200)^o$ reflections while the $(001)^m$ reflection appears only at the outer side of the fiber. There is, however, evidence for weak scattering at the $(001)^m$ position across a larger range of sample diameter. This may be due to a band of monoclinic phase extending around the circumference of the fiber, although some bulk contribution or diffuse scattering from disordered chains cannot be excluded. A difference in volume fractions of both phases should also be reflected in a difference of the radial reflection line width. Indeed one finds for the equatorial reflections $\Delta s \approx 2\text{Å}^{-1}$ fwhm (full width at half-maximum) ($s = 1/d$) for the orthorhombic

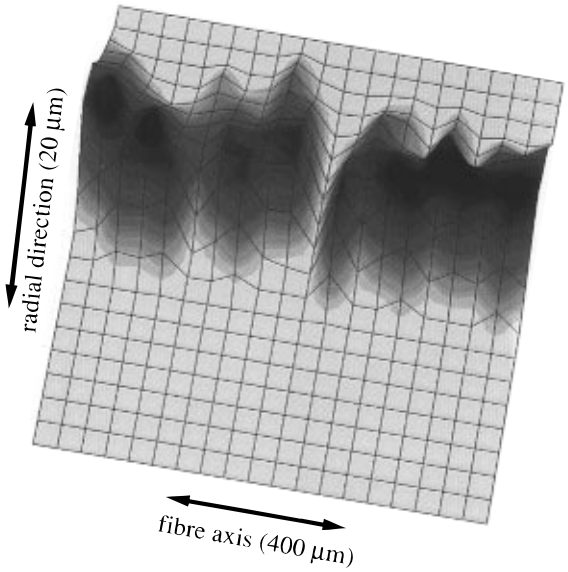

Figure 6. Pseudo-3D plot of $(001)^m$ intensity in the direction of the fiber axis. Step increments, 1 μm across the fiber and 20 μm along the fiber axis.

phase and $\Delta s \approx 4\text{Å}^{-1}$ fwhm for the monoclinic phase. Figure 5b shows the variation of integrated intensities for these three reflections when stepping radially across the fiber with the 2 μm beam. The apparent fiber diameter of about 20 μm corresponds to SEM results. The extension of the monoclinic phase into the direction of the fiber axis was determined by a series of radial scans with an increment of 20 μm along the fiber axis. A pseudo 3D plot of $(001)^m$ intensity suggests the presence of at least two separate blocks within the 400 μm scanned (Figure 6). The present data do not allow, however, derivation of a model for a 3D distribution of blocks. This will require mapping of the distribution of the orthorhombic and monoclinic phases for different rotation angles around the fiber axis. Work along this line is in progress.

The transformation of orthorhombic into monoclinic polyethylene is due to plastic deformation.[13] Crystalline blocks of orthorhombic and "triclinic" phases have been observed in transmission electron diffraction (TEM) experiments on ultradrawn polyethylene foils of ≤ 1 μm thickness.[16,17] Preferred orientation effects of orthorhombic crystalline blocks were also observed by TEM.[16] In contrast, a fiber texture was observed with the 30 μm X-ray beam (see above). The observed intensity ratio $I_{110}/I_{200} = 2.8$ is in reasonable agreement with the calculated ratio of $I_{110}/I_{200} = 3.1$ for orthorhombic polyethylene[12,18] given the difficulty of separating the amorphous halo from the reflections. The variation of the I_{110}/I_{200} ratio across the fiber (Figure 5b) observed for the 2 μm beam suggests, however, that the fiber is composed out of at least two blocks which differ in preferred orientation. This implies that the size of the domain blocks is on the level of the 2 μm beam but must be smaller than 30 μm. These results suggest also that 110 planes of orthorhombic polyethylene and 001 planes of monoclinic polyethylene have a similar orientation which may explain why the change of $(001)^m$ and $(110)^o$ reflections appears to be correlated. A more detailed analysis of orientation effects will require to determine the texture across the fiber.

Kevlar 49. An SEM image of a $\approx$12 μm thick Kevlar 49 fiber is shown in Figure 7a. Figure 7b shows a WAXS pattern recorded with a 30 μm beam. The peak

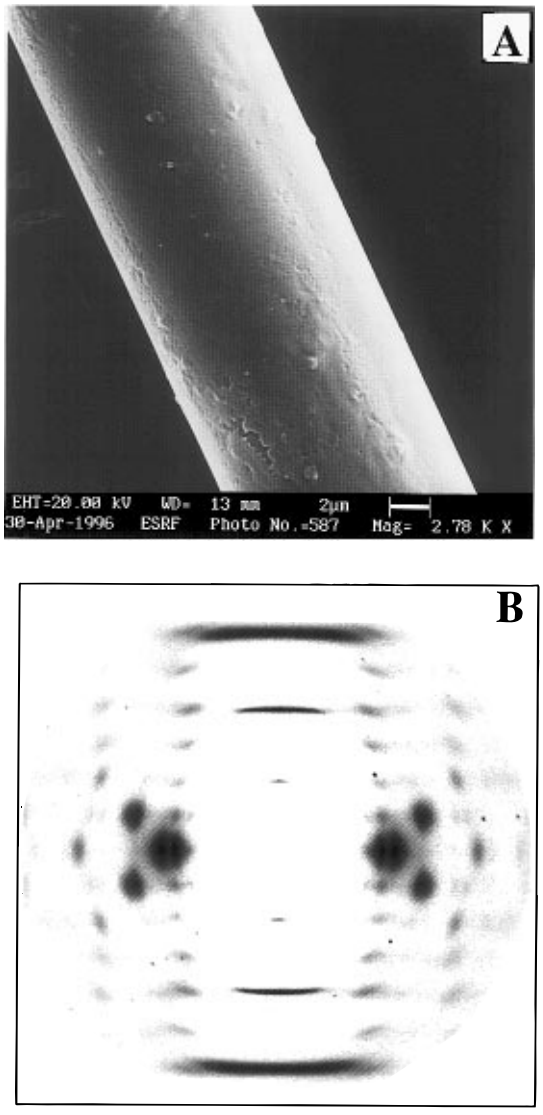

Figure 7. (a) SEM image of Kevlar 49 fiber. (b) WAXS pattern of Kevlar 49 fiber (logarithmic scale); the fiber axis is vertical.

count rate for the strongest reflection (200) is about 4600 counts/s. The sample corresponds to the Northolt polymorph[19] with a unit cell of $a = 7.86(1)$Å, $b = 5.14(6)$ Å, $c = 13.03(3)$Å, $\gamma = 90°$. As for polyethylene, no texture was observed when rotating the sample around the fiber axis.

Scanning experiments were performed in the same way as for polyethylene. A composite picture recorded with the 5 μm beam at 1 μm distance across the fiber is shown in Figure 8a. Besides the (110)/(200) reflections an equatorial streak—assumed to be due to scattering from voids[20] or crystallites in the fiber[21]—is visible. Figure 8b shows a plot of integrated intensities of both reflections this time for the 2 μm beam. The extension of scattering corresponds reasonably well to the dimension of the fiber determined by SEM.

For the sake of model calculation, two opposite, idealized models will be considered (Figure 9). Both models assume radially arranged, hydrogen-bonded sheets. The FTM (fiber texture model) assumes that the fiber is composed out of fibrils where in each fibril the sheets are radially oriented. The size of a fibril is assumed to be smaller than the 2 μm beam. Scattering with the 2 μm or the 30 μm beam should show the same fiber texture pattern. For the 2 μm beam, reflection

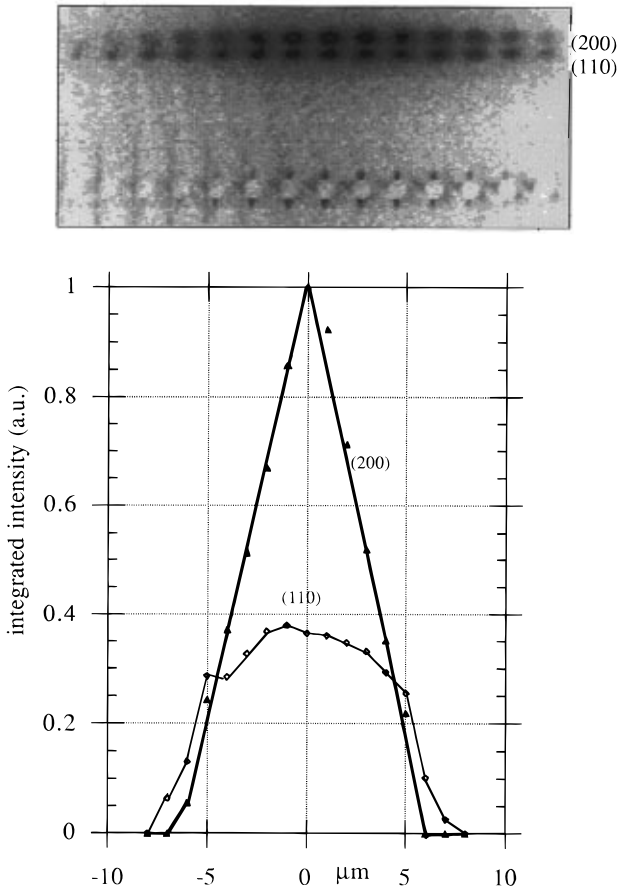

Figure 8. (a) Composite equatorial WAXS patterns of Kevlar 49 fiber with a 5 μm beam and 1 μm steps across the fiber. Due to overlapping patterns, the (006) reflection is only partially visible. (b) Variation of integrated intensities (I_{200}, I_{110}) of Kevlar 49 for 1 μm steps in the radial direction across the fiber with a 2 μm beam.

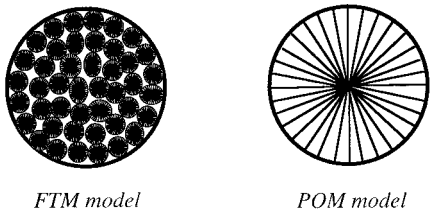

Figure 9. Looking down the fiber axis for two idealized models of a Kevlar fiber.

intensities should be proportional to the area of the fiber covered by the beam at a particular position of the fiber in the beam. The POM (preferred orientation model) is based on TEM data which suggest a continuous rotation of sheets of cells around a central axis of the fiber with *b*-axes oriented in radial direction.[22] In this case the 2 μm beam should result in local variations of relative reflection intensities due to preferred orientation effects. Figure 10 shows the scattering geometry based on this idealized model with solid lines corresponding to maximum (200) and (110) scattering. α-values are defined clockwise relative to the direct beam direction ($\alpha = 0$). The intensity of the (200) reflection will be maximized at $\alpha = \pm\Theta_{200}$ and $\alpha = 180 \pm \Theta_{200}$ where $\Theta_{200} = 7.0°$ at $\lambda = 0.96$ Å. Maximum (110) intensity will be obtained for $\alpha = \pm(\Phi_{200/110} - \Theta_{110})$ and $\alpha = 180 \pm (\Phi_{200/110} - \Phi_{110})$ where the interplanar angle $\Phi = 56.8°$ and $\Theta_{110} = 6.4°$. This allows modeling of the scattering by determining the "illuminated" length of each line as a function of the beam position on the sample.

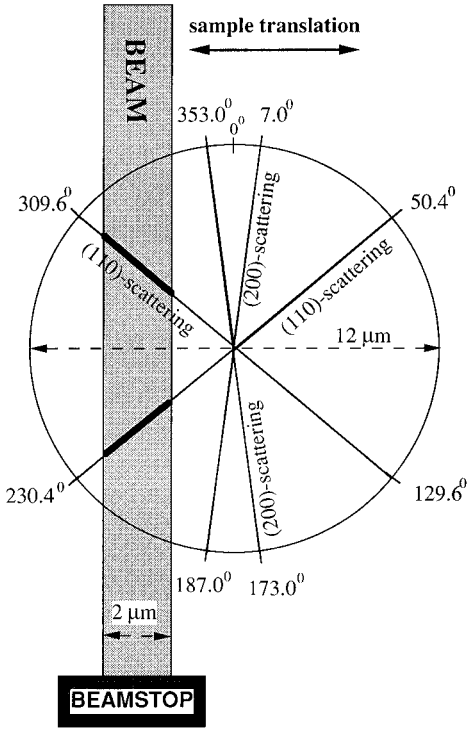

Figure 10. Geometry for scattering according to idealized radial orientation of *b*-axes around the fiber axis for POM. Solid lines correspond to orientation of *b*-axes for maximum scattering of (200) and (110) reflections. Scattering will depend on the "illuminated" length of each line by the 2 μm beam (shown as thick lines).

Figure 11a shows the variation of the illuminated area for FTM and Figure 11b the magnitude of the length of each line covered by the beam for POM multiplied by reflection multiplicities and structure factors of (110) and (200) reflections assuming a pseudoorthorhombic cell.[19] A comparison between experimental and calculated data favors POM, particularly in view of the (200) reflection. It is intereresting to note that $I_{200} > I_{110}$ for the central part and $I_{200} < I_{110}$ for the outer part of the fiber was also observed by TEM.[23] X-ray microdiffraction data suggest in addition that (200) scattering is distributed over a larger zone of the fiber as compared to the model indicated in Figure 8. This implies that the idealized *b*-axes orientation does not hold, which may be due to the the presence of crystalline blocks with an orientation distribution around the fiber axis. An imperfect microcrystalline structure has also been derived from other measurements.[23] No information on the pleated sheet structure[20] was obtained at this level of beam size. Smaller beam sizes, available at present for example with X-ray wave guides[24,25] in one direction and possibly with a new generation of glass capillaries, will be of interest in this context.

Conclusions

It is technically possible to record spatially resolved WAXS patterns from single polymeric fibers down to $\approx$10 μm thickness with a few microns beam in a few seconds per pattern. This opens new possibilities for in-situ experiments but also for the study of smaller samples. Low-angle scattering patterns can be obtained in the same way but are limited in resolution by the

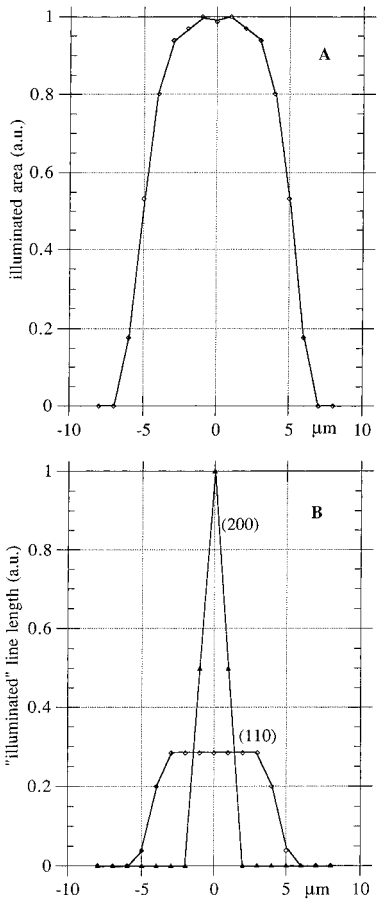

Figure 11. (a) Scattering as a function of the position of a 2 μm beam on the fiber for a model of fiber texture (FTM; see the text). Calculated values scaled to 1 at maximum. (b) Scattering as a function of the radial position of a 2 μm beam on the fiber for POM. Optimum orientation of *b*-axes for (110) and (200) scattering assumed (see Figure 10). Calculated values have been scaled according to relative intensitiy and multiplicity and scaled to 1 at a maximum of (200) scattering.

divergence of the focused beam.[4] Development has, however, just started in this area.

Acknowledgment. We would like to thank H. Chanzy for stimulating discussions, P. Engström for the provision of the capillary and Figure 2, and I. Snigireva for the SEM images.

References and Notes

(1) Bilderback, D. H.; Thiel, D. J.; Pahl, R.; Brister, K. E. *J. Synchrotron Rad*. 1994, **1**, 37.

(2) Engström, P. *Development of Capillary Optics for X-ray Focusing*, thesis, Chalmers University of Technology, Göteborg, Sweden, 1991.

(3) Riekel C.; Engström, P. *Nucl. Instrum. Method* **1995**, *B97*, 224.

(4) Engström, P.; Riekel, C. *J. Synchr. Rad*. **1996**, *3*, 97.

(5) Li, Y.; Wu, C.; Chu, B.; J. *Polym. Sci., B, Polym. Phys.* **1991**, 1309.

(6) Prasad, K.; Grubb, D. T. *J. Polym. Sci., B, Polym. Phys*. **1990**, 2199.

(7) Fankuchen, I.; Mark, H.; *J. Appl. Phys.* **1944**, *15*, 365.

(8) Engström, P.; Fiedler, S.; Riekel, C. *Rev. Sci. Instrum*. **1995**, *66* (2), 1348.

(9) Engström, P.; Riekel, C. *Rev. Sci. Instrum*. **1996**, *67* (12), 1.

(10) Mahendrasingam, A.; Martin, C.; Fuller, W.; Blundell, D. J.; MacKerron, D.; Rule, R. J.; Oldman, R. J.; Liggat, J.; Riekel, C.; Engström, P. *J. Synchr. Rad*. **1995**, *2*, 308.

(11) Hammersley A. P.; Svensson S. O.; Thompson A. *Nucl. Instr. Meth*. **1994**, *A346*, 312−321; further information via *www.esrf.fr*. FIT2D is a noncommercial crystallographic program package developed at ESRF for display and manipulation of 2D detector data. The program package is available under certain conditions to outside users.

(12) Tadokoro, H. *Structure of Crystalline Polymers*; Robert E. Kriger Publ. Comp., Malabar, 1990.

(13) Turner-Jones, A. *J. Polym. Sci.*, **1962**, *174*, 853.

(14) Seta, T.; Hara, T.; Tanaka, K. *Jpn. J. Appl. Phys.* **1968**, *7*, 31.

(15) Grubb, D. T..; Prasad, K. *ACS Polym. Symp*. **1992**, *33*, 302.

(16) Chanzy, H. D.; Smith, P.; Revol, J. F.; John Manely, R. St. *Polym. Commun*. **1987**, *28*, 133.

(17) Smith, P.; Boudet, A.; Chanzy, H. *J. Mat. Sci. Lett*. **1985**, *4*, 13.

(18) Dorset, D. L. *Polymer* **1986**, 1347.

(19) Northolt, M. G. *Eur. Polym. J*. **1974**, *10*, 799.

(20) Dobb, M. G.; Johnson, D. J.; Saville, B. P. *Polymer* **1979**, *20*, 1284.

(21) Grubb, D. T. Prasad, K.; Adams, W. *Polymer* **1991**, *32*, 1167.

(22) Dobb, M. G.; Johnson, D. J.; Saville, B. P. *J. Polym. Sci., Phys.* **1977**, *15*, 2201.

(23) Jackson, C. L.; Schadt, R. J.; Gardner, K. H.; Chase, D. B.; Allen, S. R.; Gabara, V.; English, A. D. *Polymer* **1994**, (6), 1123.

(24) Lagomarsino, S.; Jark, W.; DiFonzo, S.; Cedola, A.; Mueller, B.; Engström, P.; Riekel, C. *J. Appl. Phys.* **1996**, *79* (8), 1.

(25) Feng, Y. R.; Sinha, S. K.; Fullerton, E. E.; Grübel, G.; Abernathy, D.; Siddons, D. P.;Hastings, J. B. *Appl. Phys. Lett.* **1995**, *24*, 3647.

MA960799S